

Vogel-Fulcher-Tamman Freezing of a Thermally Fluctuating Artificial Spin Ice Probed by X-ray Photon Correlation Spectroscopy

S. A. Morley,^{1,*} D. Alba Venero,² J. M. Porro,² S. T. Riley,³ A. Stein,⁴
P. Steadman,⁵ R. L. Stamps,⁶ S. Langridge,² and C. H. Marrows^{1,†}

¹*School of Physics and Astronomy, University of Leeds, Leeds LS2 9JT, United Kingdom*

²*ISIS, STFC Rutherford Appleton Laboratory, Chilton, Didcot OX11 0QX, United Kingdom*

³*School of Electronic and Electrical Engineering,*

University of Leeds, Leeds LS2 9JT, United Kingdom

⁴*Center for Functional Nanomaterials, Brookhaven National Laboratory, Upton, New York 11973, USA*

⁵*Diamond Light Source, Chilton, Didcot OX11 0DE, United Kingdom*

⁶*SUPA, School of Physics and Astronomy, University of Glasgow, Glasgow G12 8QQ, United Kingdom*

(Dated: December 3, 2024)

We report on the crossover from the thermal to athermal regime of an artificial spin ice formed from a square array of magnetic islands whose lateral size, $30 \text{ nm} \times 70 \text{ nm}$, is small enough that they are superparamagnetic at room temperature. We used resonant magnetic soft x-ray photon correlation spectroscopy (XPCS) as a method to observe the time-time correlations of the fluctuating magnetic configurations of spin ice during cooling, which are found to slow abruptly as a freezing temperature $T_0 = 178 \pm 5 \text{ K}$ is approached. This slowing is well-described by a Vogel-Fulcher-Tamman law, implying that the frozen state is glassy, with the freezing temperature being commensurate with the strength of magnetostatic interaction energies in the array. The activation temperature, $T_A = 40 \pm 10 \text{ K}$, is much less than that expected from a Stoner-Wohlfarth coherent rotation model. Zero-field-cooled/field-cooled magnetometry reveals a freeing up of fluctuations of states within islands above this temperature, caused by variation in the local magnetic field configurations. This Vogel-Fulcher-Tamman behavior implies that the system enters a glassy state on freezing, which is unexpected for a system with a well-defined ground state.

PACS numbers: 75.40.Gb, 75.50.Tt, 05.40.-a

In the past decade a new species of magnetic metamaterials has emerged: the artificial spin ices (ASI) [1, 2]. They consist of a 2-dimensional array of nanoscale magnetic islands arranged so that the magnetostatic interactions between the islands are geometrically frustrated [3]. The size and shape of the individual islands are designed with the intention that their shape anisotropy means they act as single-domain Ising-like macropins, mimicking the atomic spins of their naturally-occurring 3-dimensional analogs [4–6], but confined to a plane. They are thus realizations of the square ice vertex models solved by Wu [7] and Lieb [8], in which the exact microstate of the statistical mechanical system can be inspected using advanced microscopy methods. Until very recently, all ASIs studied have been athermal—albeit showing an effective thermodynamics [9–12]—since the shape anisotropy energy barrier E_A that must be surmounted to flip the magnetic moment of any one island is orders of magnitude larger than any thermal energy $k_B T$ that can be reached experimentally. Whilst convenient for imaging studies, these athermal, arrested systems lack ergodicity and so fail to explore phase space in the manner of a true statistical mechanical system to find thermally equilibrated configurations.

However, there are recent reports of thermalized ASIs, made either by heating the sample close to the Curie point of the material from which the islands are fabricated in order to drive dynamics [13], whereupon the

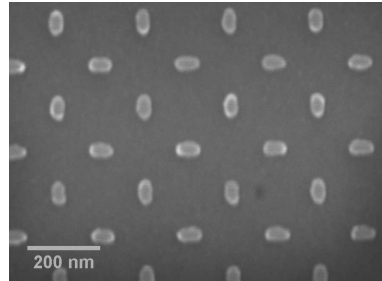


FIG. 1. Scanning electron micrograph of an artificial spin ice with a lattice spacing of 240 nm, with Permalloy islands of lateral size $30 \text{ nm} \times 70 \text{ nm}$ and 8 nm thickness.

arrested state may be imaged upon cooling [14, 15], or a one-shot anneal process that occurs during fabrication has been used in the same way [16]. Within the last year or two, studies have been carried out that have dynamically imaged real-time thermal fluctuations in artificial spin ice in the square [17], kagomé [18, 19], and tetris ice geometries [20]. Nevertheless the nature of the crossover from a thermally fluctuating system to the arrested, less ergodic state has so far received little attention. Here we report on measurements of an ASI with islands of lateral size $30 \text{ nm} \times 70 \text{ nm}$ [21], shown in Fig. 1. By studying the time-dependence of their soft x-ray speckle scattering patterns, the ASI is shown to be thermal at room temperature and to freeze into a fully arrested state below

~ 178 K. The fluctuation rate follows a Vogel-Fulcher-Tammann law on cooling, implying that the frozen state is glassy in nature, which is unexpected for a system with a well-defined ground state.

The ASI that we studied was fabricated using electron beam lithography with a lattice constant of 240 nm, as shown in Fig. 1. A lift-off process was used, with 8 nm thick Permalloy (Ni₈₀Fe₂₀) evaporated through the resist mask to form the islands, followed by a 2 nm Al cap. The substrate was a Si wafer. The ASI array had a 2 mm \times 2 mm area. Soft x-ray photon correlation spectroscopy (XPCS) coherent scattering measurements were carried out at the I10 beamline at Diamond in order to measure the time-time correlations of the magnetic fluctuations in the ASI. The experiments were carried out using circularly polarized light at the Fe L_3 (707 eV) resonance. The scattered intensity from the ASI was recorded in the reflection geometry (illustrated in Fig. 2(a)) using a charge coupled device (CCD) camera, mounted at a fixed scattering angle $2\theta = 9.6^\circ$, 80 cm from the sample, which was kept at a temperature of 223 K in order to reduce dark noise. Each image arose from a 40 ms exposure and the images were separated by the 4 s readout time of the camera. The transverse coherence length of the beam was calculated to be 14.9 μm , and so a 10 μm diameter pinhole was mounted 23 cm in front of the sample. Airy rings were observed when the direct beam was imaged through the pinhole, shown in Fig. 2(b), confirming the coherence of the beam. The samples were mounted for measurement on a temperature-controlled stage in the absence of any applied magnetic field.

Since our ASI array has a square unit cell, it produces a square pattern of diffraction spots. In Fig. 2, the centre of the diffracted speckle pattern corresponds to $Q_x = 2\pi/a$, where a is the ASI lattice constant. The calculated lattice spacing for the ASI measured from the position on the array detector and the geometry was 239 ± 2 nm, which agrees with that measured from SEM, 243 ± 4 nm. In previous scattering experiments on square ASIs incoherent light has been used to determine the different sublattice contributions to the hysteresis measured on different orders of diffraction [22] or to observe half order magnetic ground state peaks from as-grown samples [23]. When coherent illumination is used then the diffraction spot decomposes into speckle, arising from the disorder in the illuminated region of the sample introducing different phase shifts into the scattered waves [24]: this speckle is visible in the detailed views of the diffraction spots shown at the top of Fig. 2(a). The crux of the XPCS technique is that dynamics in the magnetic configuration is reflected in changes in the details of the speckle pattern. This effect has long been used with light at visible wavelengths to study relaxation and aging phenomena in soft matter [25]. XPCS experiments utilising hard x-rays have been used to study charge density waves associated with antiferromagnetic domains in Cr [26], giving an in-

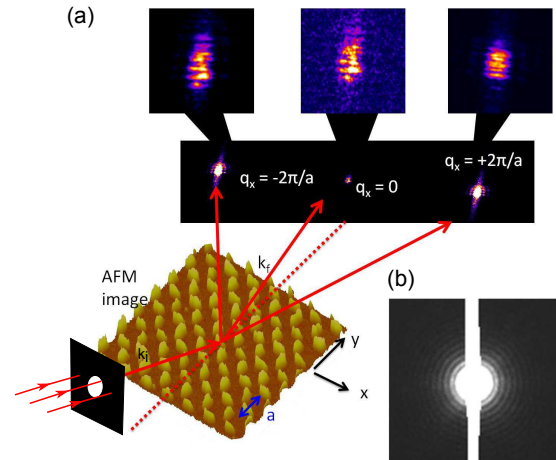


FIG. 2. (Color online) Coherent soft x-ray scattering measurements. (a) Schematic of the experimental XPCS setup, showing the incoming x-ray beam and scattered beams from the ASI array, which is represented by an atomic force microscopy image. The three main diffraction spots in the row above the specular reflection are shown here. Since the diffraction spots arise from a small, disordered region of the sample that has been coherently illuminated, they contain speckle contrast. (b) Fraunhofer diffraction obtained using the 10 μm pin hole and straight-through beam on to the CCD detector.

direct measurement of magnetic dynamics. Soft x-rays at the M_5 resonance of Ho revealed antiferromagnetic domain fluctuations in a thin film of that metal [27], whilst the jamming of spiral magnetic domains in a Y-Dy-Y trilayer was revealed in the stretched exponential correlations studied using soft X-rays at the Dy M_5 resonance [28]. There have also been speckle scattering studies at the Co L_3 resonance using small-angle X-ray scattering geometry to study the effects of disorder on the domain pattern of multilayer perpendicular Co/Pt films in response to a field [29].

As expected, measurements taken at an energy of 700 eV, below the Fe L_3 resonance, showed no change beyond random noise fluctuations (see Supplementary Movie 1), since the ASI physical structure is static. On tuning to the L_3 resonance at 709 eV, magnetic sensitivity is achieved and the speckle reconfigures as time passes, since the magnetic state of the sample is reconfiguring under thermal activity (see Supplementary Movie 2). The XPCS measurements were carried out at different temperatures to drive the thermal fluctuations at different rates. In order to quantify the time-dependent behaviour, we calculated the intensity-intensity temporal autocorrelation function [25],

$$g_2(\mathbf{Q}, \tau) = \frac{\langle I(\mathbf{Q}, t') I(\mathbf{Q}, t' + \tau) \rangle_{t'}}{\langle I(\mathbf{Q}, t')^2 \rangle_{t'}} = 1 + A |F(\mathbf{Q}, \tau)|^2, \quad (1)$$

where $I(\mathbf{Q}, t')$ is the intensity at wave vector \mathbf{Q} at a time t' , τ is the time delay, and $\langle \dots \rangle_{t'}$ indicates a time av-

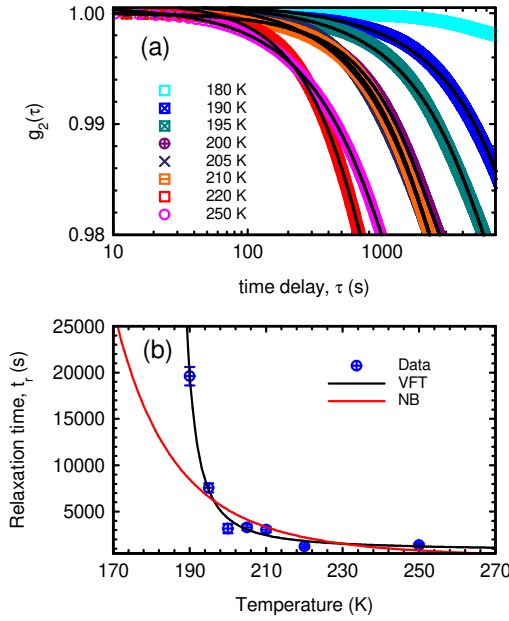


FIG. 3. (Color online) XPCS results. (a) Normalized $g_2(\tau)$ functions at various temperatures. The lines are fits to Eq. 2. (b) Relaxation times t_r as a function of temperature, fitted by a Vogel-Fulcher-Tammann (VFT) law. Also plotted is the superparamagnetic Néel-Brown (NB) law, which fits poorly.

erage. $F(\mathbf{Q}, t')$ is the so-called intermediate scattering function, and A is a measure of the degree of speckle contrast. The g_2 function was calculated for each pixel within the speckle pattern of the Bragg peak, and averaged over all such pixels to give the autocorrelation $g_2(\tau)$ at each temperature, shown normalized to an initial value in Fig. 3(a).

These $g_2(\tau)$ curves were fitted with a heterodyne model, since the experimental setup means that the fluctuating magnetic signal is mixed with a static signal that comes from the structural scattering from the array [30]. This forms the equivalent of a reference beam in the measurement, leading to the following modified form of the Kohlrausch-Williams-Watts [31, 32] intermediate scattering function [33]:

$$g_2(\tau) = 1 + A \cos(\omega\tau) \exp(-(\tau/t_r)^\beta) \quad (2)$$

where t_r is the characteristic relaxation time, β is a stretching exponent, and ω is an oscillation frequency associated with the heterodyne mixing. The value of ω was found to be in the range $\approx 0.001\text{-}0.002 \text{ rads}^{-1}$, corresponding to a time period, $2\pi/\omega = 3,140\text{-}15,700 \text{ s} (\approx 1\text{-}4 \text{ hrs})$, which correlates well with the total measurement time. The speckle contrast coefficient, A , was found to be in the range $0.02\text{-}0.05$, which agrees with that found from the contrast of the Airy pattern [34]. The fitted value of β in all our measurements was 1.0 ± 0.1 , indicating equilibrated behavior [26]. The function is rather flat at 180 K, and therefore the relaxation time must be

much longer than the time of measurement ($\approx 3 \text{ hrs}$) at that temperature, and so cannot be accurately determined. The correlation function drops off more and more quickly with increasing temperature, as can be seen from the initial slope and the drop-off in Fig. 3(a). At room temperature the system fluctuates too quickly and the speckle appears blurred due to the insufficient time resolution of our CCD acquisition.

For temperatures between 190 and 250 K, t_r lies in the experimentally accessible range between these two extremes, shown in Fig. 3b. The simplest thermal activation behavior in a collection of magnetic nanoparticles is the Arrhenius-type Néel-Brown (NB) law expected for a non-interacting superparamagnetic system, $t_r = \tau_0 \exp(T_A/T)$, where $T_A = E_A/k_B$ is an activation temperature and τ_0 is an activation time. As can be seen in the figure, this cannot be fitted to the data at all well. On the other hand, a Vogel-Fulcher-Tammann (VFT) law [35–37] captures the low temperature detail much more accurately: the data were fitted with the expression

$$t_r = \tau_0 \exp\left(\frac{T_A}{T - T_0}\right), \quad (3)$$

where T_0 is the freezing temperature. The fit yields $T_A = 40 \pm 10 \text{ K}$ and $T_0 = 178 \pm 5 \text{ K}$.

The defining feature of a VFT law is the freezing temperature T_0 , below which interactions in the system prevent any relaxation or fluctuation. Whilst the VFT law has been found to fit many different types of data sets very well, such as spin glasses, super-cooled organic liquids, metallic liquids, and glassy (bio)polymer systems [38, 39], it is nevertheless an empirical law not based on any underlying microscopic picture. Models that attempt to provide a VFT-like temperature dependence include—among others—ones based on a time-dependent percolation process [39], or on the energy depth distribution of the depth of coupled traps [40]. In the spin glass theory of Shtrikman and Wohlfarth (S-W) [41], the random exchange interactions between the positionally disordered spins are represented by a mean magnetic interaction field H_i . The magnetostatic interactions in our ASI are real magnetic fields, making the S-W theory a natural one to adapt to our system. In it, the freezing temperature T_0 is determined by the characteristic interaction energy E_i . Using the results from the VFT fit, we find $E_i = \sqrt{k_B^2 T_0 T_A} \approx 1.2 \times 10^{-21} \text{ J}$.

We can estimate the scale of magnetostatic interactions in our ASI using a point dipole model to determine the S-W interaction energy:

$$E_i = \mu_0 H_i m_{\text{island}} = \frac{\mu_0 m_{\text{island}}^2}{2\pi a^3}, \quad (4)$$

where $m_{\text{island}} = M_s V$ is the magnetic moment of an island of volume V and the lattice constant $a = 240 \text{ nm}$. Assuming the nominal island size and the bulk magnetization of Permalloy ($M_s = 860 \text{ kA/m}$) yields $E_i =$

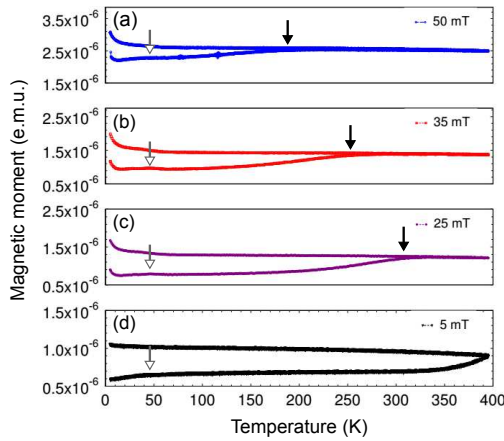


FIG. 4. (Color online) ZFC and FC magnetization measurements under different applied magnetic probe fields of (a) 50 mT, (b) 35 mT, (c) 25 mT and (d) 5 mT. The black arrow indicates the temperature at which the curves bifurcate, the grey arrow the low temperature feature. The field is applied along [01] direction of the ASI lattice.

3.0×10^{-21} J, which is of the same order of magnitude as the experimental value but overestimated by about a factor of three. Part of the overestimate may be due to the extrinsic effect of the reduction in effective M_s [19] or V [42] due to oxidation. An intrinsic contribution to the overestimate is the fact that the total interaction energy arises from the sum of several frustrated interactions from all the island's neighbors, leading to partial cancellation of the energy value given above. Thus, the magnetostatic interactions in the system are clearly of the right scale to break the Arrhenius-like behaviour and give rise to a VFT-like freezing of the fluctuations as T_0 is approached.

Now we turn to discussion of the activation temperature T_A . We can estimate the energy barrier ΔE for Stoner-Wohlfarth coherent rotation of a single island, again assuming the bulk magnetization of Permalloy, using $\Delta E = KV = \ln(f_0 t_m) k_B T_A$, with the shape anisotropy constant $K = \frac{1}{2} \mu_0 \Delta D M^2$, and the difference in demagnetizing factor along the two relevant directions $\Delta D \approx 0.1$ based on the island geometry [43]. Here the measurement time, t_m , is taken as two hours, a typical value for $2\pi/\omega$, and we assume $f_0 = 10$ GHz. This yields $T_A \approx 1700$ K. This is far larger than the fitted T_A of 40 K, ruling out this simple picture.

In order to seek other evidence of thermally-activated processes that might cast light on this large discrepancy, standard zero-field cooled (ZFC) and field-cooled (FC) protocols were carried out on the samples using SQUID-vibrating sample magnetometry. First, the sample was heated to 395 K and a large negative saturating field applied and removed. The sample was then cooled to 5 K without any applied field. Next, a probe field was

applied and the magnetic moment was measured during heating, which is the lower curve in each measurement in Fig. 4. Last, the sample was measured again during cooling back down with the probe field still applied. The peak in the ZFC, close to where the curves bifurcate is the blocking temperature T_B , marked with a black arrow. For the data with probe field $\mu_0 H = 50$ mT, $T_B(50 \text{ mT}) = 200 \pm 10$ K. The blocking temperature systematically becomes lower for larger probe fields. This behavior can be extrapolated to the case where there would be zero applied probe field, using $T_B \propto H^{2/3}$ [44], which gives $T_B(0 \text{ mT}) = 460 \pm 20$ K. This is about a factor of four lower than that expected from the sample parameters and nominal volume. Whilst reduced magnetization or volume can explain some of this discrepancy, it is seems clear once again that a pure coherent rotation mechanism is not strictly followed.

Nevertheless, there is another feature in the magnetometry data for the 5 mT probe field: there is an initial increase in moment up to 40 K, marked with a open arrow arrow, with weaker features in the other curves also appearing. This signifies a much lower energy scale for some magnetic relaxation process, one that is strikingly similar to the T_A found from the VFT fit. The appearance of this 40 K feature has the remarkable property that it is dependent on the angle of the magnetic field applied. As is shown in Fig. 5(a) the feature is only seen when the field is along the [01] direction of the array and is absent when the field is along the [11] direction. This is to be expected from a consideration of the local field exerted on a given island from its neighbors (see Fig. 5(b) and (c)). When magnetised along [11], the local field direction is well-defined for every island. On the other hand, when the field is along [01] it magnetises one sublattice of the square array but different configurations are possible for islands with their easy axis perpendicular to the applied field, leading to a range of different local field configurations. Nanoscale magnetic islands such as ours are not perfect single domains but tend to display deviations from uniformity at their ends which are metastable and form overall micromagnetic configurations known as C- or S-states [45], which can display enhanced fluctuations in these varying local fields. This ability to control the degree of variation in the local fields is unique to this type of lithographically-defined array and is not possible with conventional fine particle magnetic systems, in which local field variations are always present.

As previously shown by Ozatay et al. [46], the properties of Py can change below 40 K when native oxidation occurs. They showed in elements of a similar size that such oxidation is likely around the unprotected edges and can have significant effects on the reversal properties. They attribute this to the local anisotropy from the exchange coupling with the antiferromagnetic oxide edges which allows non-uniform modes to reversal to become energetically accessible. This can create a random

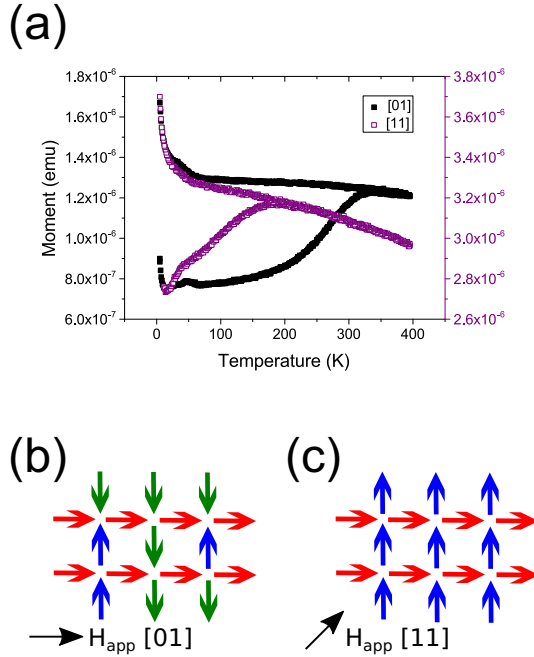


FIG. 5. (Color online) Angle dependence of the field direction. (a) The ZFC-FC protocol carried out with a probe field of 25 mT applied along the [01] direction (as shown in Fig.4 (solid squares), with a peak at low temperature. Also shown is the same measurement with the field applied equally to all array elements i.e. along the [11] direction (open squares). In that case, the peak is suppressed as the local field variations are removed. (b) A spin ice magnetised along the [01] direction has a variety of different local field configurations around the elements magnetised along the field direction (red arrows). (c) When magnetised along the [11] direction, every island experiences an identical local field environment.

distribution of local anisotropy axes, this along with a distribution of local fields allows the system to sample a distribution of metastable states only once a temperature of $T_A = 40$ K is exceeded.

To summarize, on cooling an artificial spin ice we have observed a dramatic lengthening of the relaxation time. The system slows abruptly as it crosses over from thermal equilibration to an athermal, frozen state. This crossover can be described by a Vogel-Fulcher-Tamman law, which typically describes glassy systems. The freezing temperature $T_0 \approx 178$ K is in good accord with the magnetostatic interaction strength. The activation temperature $T_A \approx 40$ K arising from a fit of this law implies a much lower energy barrier to reversal than is expected from a single-domain coherent rotation picture. The value of 40 K appears to be determined by the onset of fluctuating magnetic states within the islands coupled to magnetic oxides at the edges of the islands. Our ZFC/FC data under different field directions show that these fluctuations are only significant in the presence of randomly varying local field configurations experienced by the islands. In the XPCS experiments, which are

performed at remanence, a large proportion of the islands will experience such varying local field configurations, and so these fluctuations can take place, leading to the observed T_A . The glass-like freezing is remarkable since the square ice system possesses a well-defined ground state, unlike a conventional spin glass. This raises the question of the nature of the glassy state. Related VFT-like freezing behaviour has recently been observed in the pyrochlore spin ice $Dy_2Ti_2O_7$ [47], prompting speculation about this representing many-body localization of spins in a translationally-invariant quantum system [48–50]. This is unlikely to be the case here since the artificial systems of the type we have studied consist of classical macrospins, implying that some other unusual glass state is obtained in these samples once ergodicity is broken.

This work was supported by the EPSRC (grant numbers EP/J021482/1 and EP/I000933/1). Research carried out in part at the Center for Functional Nanomaterials, Brookhaven National Laboratory, which is supported by the U.S. Department of Energy, Office of Basic Energy Sciences, under Contract No. DE-AC02-98CH10886. We would like to thank S. S. Dhesi for the loan of the CCD camera.

* Email: S.A.Morley@leeds.ac.uk

† Email: C.H.Marrows@leeds.ac.uk

- [1] C. Nisoli, R. Moessner, and P. Schiffer, “Colloquium: Artificial spin ice: Designing and imaging magnetic frustration,” *Rev. Mod. Phys.* **85**, 1473 (2013).
- [2] L. J. Heyderman and R. L. Stamps, “Artificial ferroic systems: novel functionality from structure, interactions and dynamics,” *J. Phys.: Cond. Matt.* **25**, 363201 (2013).
- [3] R. F. Wang, C. Nisoli, R. S. Freitas, J. Li, W. McConville, B. J. Cooley, M. S. Lund, N. Samarth, C. Leighton, V. H. Crespi, and P. Schiffer, “Artificial ‘spin ice’ in a geometrically frustrated lattice of nanoscale ferromagnetic islands,” *Nature (London)* **439**, 303 (2006).
- [4] S. T. Bramwell and M. J. P. Gingras, “Spin ice state in frustrated magnetic pyrochlore materials,” *Science* **294**, 1495 (2001).
- [5] A. P. Ramirez, A. Hayashi, R. J. Cava, R. Siddharthan, and B. S. Shastry, “Zero-point entropy in ‘spin ice’,” *Nature (London)* **399**, 333 (1999).
- [6] C. Castelnovo, R. Moessner, and S. L. Sondhi, “Magnetic monopoles in spin ice,” *Nature (London)* **451**, 42 (2008).
- [7] F. Y. Wu, “Exactly soluble model of the ferroelectric phase transition in two dimensions,” *Phys. Rev. Lett.* **18**, 605 (1967).
- [8] E. H. Lieb, “Exact solution of the problem of the entropy of two-dimensional ice,” *Phys. Rev. Lett.* **18**, 692 (1967).
- [9] C. Nisoli, R. Wang, J. Li, W. F. McConville, P. E. Lammer, P. Schiffer, and V. H. Crespi, “Ground state lost but degeneracy found: The effective thermodynamics of artificial spin ice,” *Phys. Rev. Lett.* **98**, 217203 (2007).
- [10] C. Nisoli, J. Li, X. Ke, D. Garand, P. Schiffer, and V. H. Crespi, “Effective temperature in an interacting vertex system: Theory and experiment on artificial spin ice,”

Phys. Rev. Lett. **105**, 047205 (2010).

[11] P. E. Lammert, X. Ke, J. Li, C. Nisoli, D. M. Garand, V. H. Crespi, and P. Schiffer, “Direct entropy determination and application to artificial spin ice,” Nature Phys. **6**, 786 (2010).

[12] J. P. Morgan, J. Akerman, A. Stein, C. Phatak, R. M. L. Evans, S. Langridge, and C. H. Marrows, “Real and effective thermal equilibrium in artificial square spin ices,” Phys. Rev. B **87**, 024405 (2013).

[13] V. Kapaklis, U. B. Arnalds, A. Harman-Clarke, E. Th. Papaioannou, M. Karimipour, P. Korelis, A. Taromi, P. C. W. Holdsworth, S. T. Bramwell, and B. Hjörvarsson, “Melting aritificial spin ice,” New J. Phys. **14**, 035009 (2012).

[14] J. M. Porro, A. Bedoya-Pinto, A. Berger, and P. Vavassori, “Exploring thermally induced states in square artificial spin-ice arrays.” New J. Phys. **15**, 055012 (2013).

[15] S. Zhang, I. Gilbert, C. Nisoli, G.-W. Chern, M. J. Erickson, L. O’Brien, C. Leighton, P. E. Lammert, V. H. Crespi, and P. Schiffer, “Crystallites of magnetic charges in artificial spin ice,” Nature (London) **500**, 553 (2013).

[16] J. P. Morgan, A. Stein, S. Langridge, and C. H. Marrows, “Thermal ground-state ordering and elementary excitations in artificial magnetic square ice,” Nature Phys. **7**, 75 (2011).

[17] A. Farhan, P. M. Derlet, A. Kleibert, A. Balan, R. V. Chopdekar, M. Wyss, J. Perron, A. Scholl, F. Nolting, and L. J. Heyderman, “Direct observation of thermal relaxation in artificial spin ice,” Phys. Rev. Lett. **111**, 057204 (2013).

[18] A. Farhan, P. M. Derlet, A. Kleibert, A. Balan, R. V. Chopdekar, M. Wyss, L. Anghinolfi, F. Nolting, and L. J. Heyderman, “Exploring hyper-cubic energy landscapes in thermally active finite artificial spin-ice systems,” Nature Phys. **9**, 375 (2013).

[19] V. Kapaklis, U. B. Arnalds, A. Farhan, R. V. Chopdekar, A. Balan, A. Scholl, L. J. Heyderman, and B. Hjörvarsson, “Thermal fluctuations in artificial spin ice,” Nature Nanotech. **9**, 514 (2014).

[20] I. Gilbert, Y. Lao, I. Carrasquillo, L. O'Brien, J. D. Watt, M. Manno, C. Leighton, A. Scholl, C. Nisoli, and P. Schiffer, “Emergent reduced dimensionality by vertex frustration in artificial spin ice,” Nature Phys. **12**, 162 (2015).

[21] S. A. Morley, A. Stein, M. C. Rosamond, D. Alba Venero, A. Hrabec, P. M. Shepley, M.-Y. Im, P. Fischer, M. T. Bryan, D. A. Allwood, P. Steadman, S. Langridge, and C. H. Marrows, “Temperature and magnetic-field driven dynamics in artificial magnetic square ice,” Proc. SPIE **9551**, 95511Q (2015).

[22] J. P. Morgan, C. J. Kinane, T. R. Charlton, A. Stein, C. Sánchez-Hanke, D. A. Arena, S. Langridge, and C. H. Marrows, “Magnetic hysteresis of an artificial square ice studied by in-plane Bragg x-ray resonant magnetic scattering,” AIP Advances **2**, 022163 (2012).

[23] J. Perron, L. Anghinolfi, B. Tudu, N. Jaouen, J.-M. Tonnerre, M. Sacchi, F. Nolting, J. Lüning, and L. J. Heyderman, “Extended reciprocal space observation of artificial spin ice with x-ray resonant magnetic scattering,” Phys. Rev. B **88**, 214424 (2013).

[24] M. Sutton, S. G. J. Mochrie, T. Greytak, S. E. Nagler, L. E. Berman, G. A. Held, and G. B. Stephenson, “Observation of speckle by diffraction with coherent x-rays,” Nature (London) **352**, 608 (1991).

[25] Luca Cipelletti, Laurence Ramos, S. Manley, E. Pitard, D. A. Weitz, Eugene E. Pashkovski, and Marie Johansson, “Universal non-diffusive slow dynamics in aging soft matter,” Faraday Discuss. **123**, 237 (2003).

[26] O. G. Shpyrko, E. D. Isaacs, J. M. Logan, Y. Feng, G. Aeppli, R. Jaramillo, H. C. Kim, T. F. Rosenbaum, P. Zschack, M. Sprung, S. Narayanan, and A. R. Sandy, “Direct measurement of antiferromagnetic domain fluctuations,” Nature (London) **447**, 68 (2007).

[27] S. Konings, C. Schüßler-Langeheine, H. Ott, E. Weschke, E. Schierle, H. Zabel, and J. B. Goedkoop, “Magnetic domain fluctuations in an antiferromagnetic film observed with coherent resonant soft x-ray scattering,” Phys. Rev. Lett. **106**, 077402 (2011).

[28] S.-W. Chen, H. Guo, K. A. Seu, K. Dumesnil, S. Roy, and S. K. Sinha, “Jamming behavior of domains in a spiral antiferromagnetic system,” Phys. Rev. Lett. **110**, 217201 (2013).

[29] M. S. Pierce, C. R. Buechler, L. B. Sorensen, S. D. Keaveny, E. A. Jagla, J. M. Deutsch, T. Mai, O. Narayan, J. E. Davies, Kai Liu, G. T. Zimanyi, H. G. Katzgraber, O. Hellwig, E. E. Fullerton, P. Fischer, and J. B. Kortright, “Disorder-induced magnetic memory: Experiments and theories,” Phys. Rev. B **75**, 144406 (2007).

[30] Sunil K. Sinha, Zhang Jiang, and Laurence B. Lurio, “X-ray Photon Correlation Spectroscopy Studies of Surfaces and Thin Films,” Advanced Materials **26**, 7764–7785 (2014).

[31] R. Kohlrausch, “Theorie des elektrischen rückstandes in der leidner flasche,” Ann. Phys. Chemie (Poggendorff) **91**, 179 (1854).

[32] G. Williams and D. C. Watts, “Non-symmetrical dielectric relaxation behavior arising from a simple empirical decay function,” Trans. Faraday Soc. **66** (1970).

[33] F. Livet, F. Bley, F. Ehrburger-Dolle, I. Morfin, E. Geissler, and M. Sutton, “X-ray intensity fluctuation spectroscopy by heterodyne detection,” J. Sync. Rad. **13**, 453 (2006).

[34] G. Beutier, A. Marty, F. Livet, G. van der Laan, S. Stanescu, and P. Bencok, “Soft x-ray coherent scattering: Instrument and methods at ESRF ID08,” Rev. Sci. Inst. **78**, 093901 (2007).

[35] H. Vogel, “Das Temperatur-abhängigkeitgesetz der Viskosität von Flüssigkeiten (The law of temperature dependence of the viscosity of fluids),” Phys. Z. **22**, 645 (1921).

[36] G. S. Fulcher, “Analysis of recent measurements of the viscosity of glasses,” J. Am. Ceram. Soc. **8**, 339 (1925).

[37] G. Tammann and W. Hesse, “Die Abhängigkeit der Viskosität von der Temperatur bei unterkühlten flüssigkeiten (The dependence of viscosity on temperature for under-cooled fluids),” Z. Anorg. Allg. Chem. **156**, 245 (1926).

[38] C. A. Angell, “Formation of glasses from liquids and biopolymers,” Science **267**, 1924 (1995).

[39] M. Cyrot, “A possible origin for the Vogel-Fulcher law,” Phys. Lett. A **83**, 275 (1981).

[40] J.-P. Bouchaud, A. Comtet, and C. Monthus, “On a dynamical model of glasses,” Journal de Physique I France **5**, 1521 (1995).

[41] S. Shtrikman and E. P. Wohlfarth, “The theory of the Vogel-Fulcher law of spin glasses,” Phys. Lett. A **85**, 467 (1981).

[42] B. L. Le, D. W. Rench, R. Misra, L. O’Brien, C. Leighton, N. Samarth, and P. Schiffer, “Effects of exchange bias

on magnetotransport in permalloy kagome artificial spin ice,” *New J. Phys.* **17**, 023047 (2015).

[43] J. A. Osborn, “Demagnetizing factors of the general ellipsoid,” *Phys. Rev.* **67**, 351 (1945).

[44] M. El Hilo, K. O’Grady, and R. W. Chantrell, “Susceptibility phenomena in a fine particle system 2. Field-dependence of the peak,” *J. Magn. Magn. Mater.* **114**, 307 (1992).

[45] A. S. Arrott, “Introduction to micromagnetics,” (Springer, Berlin, 2005) Chap. 5, p. 101.

[46] O. Ozatay, P. G. Gowtham, K. W. Tan, J. C. Read, K. A. Mkhoyan, M. G. Thomas, G. D. Fuchs, P. M. Braganca, E. M. Ryan, K. V. Thadani, J. Silcox, D. C. Ralph, and R. A. Buhrman, “Sidewall oxide effects on spin-torque- and magnetic-field-induced reversal characteristics of thin-film nanomagnets.” *Nature Mater.* **7**, 567 (2008).

[47] E. R. Kassner, A. B. Eyyazova, B. Pichler, T. J. S. Munsie, H. A. Dabkowskac, G. M. Luke, and J. C. S. Davis, “Supercooled spin liquid state in the frustrated pyrochlore $Dy_2Ti_2O_7$,” *Proc. Nat. Acad. Sci.* **112**, 8549 (2015).

[48] W. De Roeck and F. Huveneers, “Scenario for delocalization in translation-invariant systems,” *Phys. Rev. B* **90**, 165137 (2014).

[49] N. Y. Yao, C. R. Laumann, J. I. Cirac, M. D. Lukin, and J. E. Moore, “Quasi many-body localization in translation invariant systems,” (2014), arXiv:1410.7407 [cond-mat.dis-nn].

[50] M. Schiulaz, A. Silva, and M. Müller, “Dynamics in many-body localized quantum systems without disorder,” *Phys. Rev. B* **91**, 184202 (2015).